EC
Journals.ASM.org

The Ancient Small GTPase Rab21 Functions in Intermediate Endocytic Steps in Trypanosomes

Moazzam Ali,[a]* Ka Fai Leung,[a] Mark C. Field[b]

Department of Pathology, University of Cambridge, Cambridge, United Kingdom[a]; Division of Biological Chemistry and Drug Discovery, University of Dundee, Dundee, Scotland, United Kingdom[b]

Endocytosis is an essential process in nearly all eukaryotic cells, including the African trypanosome *Trypanosoma brucei*. Endocytosis in these organisms is exclusively clathrin mediated, although several lineage-specific features indicate that precise mechanisms are distinct from those of higher eukaryotes. *T. brucei* Rab21 is a member of an ancient, pan-eukaryotic, endocytic Rab clade that is retained by trypanosomes. We show that *T. brucei* Rab21 (TbRab21) localizes to endosomes, partially colocalizing with TbRab5A, TbRab28, and TbVps23, the latter two being present at late endosomes. TbRab21 expression is essential for cellular proliferation, and its suppression results in a partial block in traffic to the lysosome. RNA interference (RNAi)-mediated knockdown of TbRab21 had no effect on TbRab5A expression or location but did result in decreased in *trans* expression of ESCRT (trypanosome endosomal sorting complex required for transport) components and TbRab28, while knockdown of ESCRT subunit TbVps23 resulted in decreased TbRab21 expression. These data suggest that TbRab21 acts downstream of TbRab5A and functions in intimate connection with the trypanosome ESCRT system.

Trypanosoma brucei is a highly divergent protozoan parasite and the causative agent of human and animal trypanosomiasis in sub-Saharan Africa. Despite a pressing need for new drugs and essentially no prospect for a vaccine, trypanosomiasis and related pathogens remain neglected by the pharmaceutical industry. *T. brucei* has emerged as a model organism for multiple pathogenic trypanosomes, including *Leishmania* and *T. cruzi*, the causative agents of leishmaniasis (kala-azar) and Chagas' disease, respectively; new therapies are urgently required for all of these pathogens. *T. brucei* is also extremely valuable for comparative cell biology, due to the phylogenetic position within the Excavata supergroup coupled with an advanced experimental toolbox. *T. brucei* is presently the most experimentally accessible member of the phylum Euglenozoa.

T. brucei evades the mammalian host acquired immune response through a combination of mechanisms, which include antigenic variation of the superabundant variant surface glycoprotein (VSG) and antibody clearance from the cell surface (discussed in reference 1). Both of these processes involve trafficking of the VSG protein through the flagellar pocket (FP), the sole site of endo- and exocytosis in these organisms. Endocytosis and recycling are extremely rapid processes and heavily reliant upon clathrin (CLH)-mediated mechanisms (2). Evolutionary modifications to the molecular machinery that subtend endocytosis include loss of the AP-2 cargo adaptor complex (3) and the presence of a cohort of lineage-specific clathrin-associated proteins (CAPs) (4). These adaptations, together with a very high endocytic flux, serve to maintain VSG surface density and rapidly remove surface-bound immune effectors, including anti-VSG antibodies (5). Further, endocytosis also contributes to mechanisms for evasion of the innate immune system that eliminate many subspecies of *T. brucei* via uptake of trypanolytic factor (TLF). Here, human or higher-primate infectivity requires modifications to endocytic and receptor-mediated internalization mechanisms (6, 7). Most recently, it has emerged that endocytosis is a major mechanism for uptake of some first-line trypanocides and that this extreme rate of endocytosis offers a potential mechanism to deliver therapeutics to the parasite in a highly efficient manner (8, 9).

Understanding the endocytic apparatus of trypanosomes is of direct therapeutic importance as well as providing insight into evolution of trafficking systems and has led to detailed characterization of several Rab proteins from this organism. Rab proteins constitute the largest family of the Ras GTPase superfamily and are important spatiotemporal regulators of membrane transport (10). Several endosomal compartments in *T. brucei* are regulated by Rab proteins and have been described by us and others. *T. brucei* Rab5A (TbRab5A)- and TbRab5B-containing endosomes receive distinct cargo in bloodstream-form (BSF) cells and, similarly to mammalian cells, are early compartments of the endocytic system (11, 12, 13). TbRab4 and TbRab11 are involved in recycling (11, 14, 15, 16, 17), and TbRab28 was recently shown to coordinate retromer-dependent trafficking and late endosomal pathways (18). TbRab7 mediates delivery from late endosomal compartments to the lysosome (19).

A Rab21 orthologue is present in trypanosomes. Significantly, Rab5, Rab20, Rab21, Rab22, Rab24, and Rab50 likely form an ancient endocytic clade that is predicted to be present in the last eukaryotic common ancestor (LECA), and thus TbRab5 and TbRab21 are the only representatives of this clade conserved in trypanosomes (20, 21). In mammalian cells, Rab21 localizes to

Received 3 October 2013 **Accepted** 20 December 2013

Published ahead of print 27 December 2013

Address correspondence to Mark C. Field, m.c.field@dundee.ac.uk.

* Present address: Moazzam Ali, Institute of Biochemistry and Biotechnology, University of the Punjab, Lahore, Pakistan.

Supplemental material for this article may be found at http://dx.doi.org/10.1128/EC.00269-13.

doi:10.1128/EC.00269-13

The authors have paid a fee to allow immediate free access to this article.

early endosomal vesicles and has extensive colocalization with early endosomal Rab4, Rab5, Rab17, and Rab22 but less with Rabs located at late and recycling endosomes. Cells expressing GTPase-inactive Rab21:T33N have defective transferrin and epidermal growth factor endocytosis and fail to deliver the latter to lysosomes (22). Rab21 localization also depends on cell polarity; Rab21 has an endoplasmic reticulum (ER)-like localization in nonpolarized mammalian cells, whereas Rab21 is present at apically located vesicles in polarized cells (23). In *Dictyostelium discoideum*, Rab21 regulates phagocytosis through physical interactions with two zinc finger LIM (Lin11, Isl-1, and Mec-3) domain proteins, LimF and ChLim (24). Inhibition of phosphoinositide-3-kinase with wortmannin induces microtubule-dependent formation of Rab21-positive tubular endosomes, which arise from Rab5 endosomes (25), while in macrophages Rab21 is transiently associated with clathrin-independent macropinosomes, being recruited downstream of Rab5 but upstream of Rab7 (26).

Rab21 is also implicated in the trafficking of integrins, metazoan-specific receptors responsible for cell adhesion, migration, maintenance of cell polarity, and cytokinesis (27, 28, 29). Rab GTPases are important regulators of integrin traffic, as Rab5 and Rab21 are important for uptake whereas Rab4 and Rab11 are involved in recycling (30, 31). However, many of these studies clearly report on lineage-specific functions, as integrins are metazoan specific and are absent from the vast majority of lineages. Beyond analysis in *D. discoideum*, essentially nothing is known of Rab21 function in nonmetazoan cells, despite the protein being an ancient representative and therefore expected to play a fundamental role in cell physiology. Here we have investigated trypanosome Rab21, both to extend our understanding of Rab21 function in nonmetazoan systems and to complete analysis of trypanosome representatives of the LECA endocytic clade. We find that *T. brucei* Rab21 localizes to endosomes and partially colocalizes with both TbRab5A and multivesicular bodies (MVBs)/late endosomes. TbRab21 expression is essential for cellular proliferation and required for traffic to the lysosome.

MATERIALS AND METHODS

Culturing of parasites. *T. brucei* bloodstream-form Lister 427 cells were cultured in HMI-9 complete medium at 37°C with 5% CO_2 in vented cap culture flasks (32). For RNA interference (RNAi) experiments, single-marker bloodstream (SMB) cells expressing T7 RNA polymerase (33) were cultured under the same conditions in the continuous presence of 5 μg/ml neomycin; expression of double-stranded RNA was induced by the addition of tetracycline at 1 μg/ml. Procycle-form (PCF) cells were cultured in SDM-79 media with 10% fetal bovine serum (FBS), L-glutamine, and hemin (34). Cells were cultured in nonvented flasks at 27°C.

Transfection of trypanosomes. *T. brucei* bloodstream-form cells were transfected with 10 μg linearized plasmids using an Amaxa Nucleofector device and an Amaxa human T cell Nucleofector kit. Individual clones of transfected cells were selected by serial dilution, using appropriate antibiotics at the following concentrations (G418, 2.5 μg/ml; hygromycin, 2.5 μg/ml; puromycin, 0.2 μg/ml). Transgenic parasites were maintained under conditions of continuous drug pressure (35). PCF cells were transfected as described previously (13).

Plasmid constructs for overexpression and RNAi. An RNAi construct against TbRab21 was made by cloning a 429-bp fragment of the *T. brucei* Rab21 open reading frame (ORF) (Tb927.10.1520), with the sequence selected using RNAit (http://trypanofan.path.cam.ac.uk/software/RNAit.html). The primers used for amplification were RNAi:Rab21:F (TGACACACTCGAGAAGGTGC) and RNAi:Rab21:R (AGATTCGCCACCTCATCATC). The amplified fragment was cloned into Eam11051 (Fermentas)-linearized p2T7-TAblue vector. This tetracycline-inducible T7 RNAi expression vector was a derivative of p2T7 (36) with blue-white screening capability. For ectopic expression, pHD1034 plasmid (37), having an rRNA promoter, was used to clone the TbRab21 gene in frame to an N-terminal yellow fluorescent protein (YFP) or hemagglutinin (HA) epitope tag to create pHD1034:Rab21. The primers used to amplify TbRab21 from genomic DNA were Rab21F (TAAAGCTTCTCGGTCGTCGGTGCCTAGT) and Rab21R (CGGATCCTCAGGAACAACAGCGGTTC). pHD1034:Rab21 was used for overexpression in both BSF and PCF cells.

qRT-PCR. Total RNA was extracted using an RNeasy Minikit (Qiagen GmbH, Germany), following the manufacturer's instructions. RNA concentrations were estimated using a NanoDrop spectrophotometer (Thermo Fisher Scientific). cDNA was synthesized using SuperScript III reverse transcriptase (Invitrogen). Real-time quantitative reverse transcription-PCR (qRT-PCR) was performed using Bio-Rad's iQ SYBR green Supermix, with 0.4 μM forward and reverse primer and cDNA equivalent to 50 to 100 ng total RNA. qRT primers were qRT:Rab21F (CGTTCCATTGCTTAACAGTGAC) and qRT:Rab21R (CACATCGTAGACGAGGATTGC). Reference genes were the genes encoding telomerase reverse transcriptase and paraflagellar rod protein 2, which were used to normalize expression using previously described primers (38) Replicate samples were assembled as a master mix with a single addition of the different templates. qPCRs were performed on a MiniOpticon real-time PCR system (Bio-Rad). The normalized expression (ΔΔ threshold cycle [C_T]) of mRNA was subsequently determined (based on one or multiple reference genes) using Bio-Rad CFX manager software.

Protein electrophoresis and Western blotting. For lysate preparation, harvested cells were washed with phosphate-buffered saline (PBS) and resuspended in SDS sample buffer before heating at 95°C for 10 min. Typically, protein samples were electrophoresed at 5×10^6 cell equivalents per lane on 10% SDS-PAGE gels and transferred to a polyvinylidene difluoride (PVDF) membrane (Immobilon; Millipore) by wet blotting using transfer buffer (192 mM glycine, 25 mM Tris, 20% [vol/vol] methanol). Ponceau S (0.1% [wt/vol] Ponceau S–5% [vol/vol] acetic acid) staining was used to monitor equivalence of transfer as well as to normalize Western blot intensities.

Western blotting was performed using standard procedures. Primary antibodies were used at the following dilutions: *T. brucei* clathrin (TbCLH), 1:2,000; TbRab5A, 1:1,000; TbRab11, 1:2,000; invariant surface glycoprotein 65 (ISG65) and ISG75, 1:10,000; TbBiP, 1:40,000; *T. brucei* transferrin receptor (TfR), 1:10,000; HA, 1:2,000; GFP, 1:20,000; FLAG, 1:1,000. Secondary antibodies (peroxidase goat anti-rabbit conjugate or peroxidase rabbit anti-mouse conjugate) were from Sigma and used at a dilution of between 1:10,000 and 1:20,000. Bound antibodies were detected by chemiluminescence using luminol and visualized by exposure to Kodak chemiluminescence film or using a G:BOX chemiluminescence imaging system from Syngene. For reprobing where needed, membranes were stripped of bound antibodies using Restore Western blot stripping buffer (Thermo Fisher Scientific). For densitometry, unsaturated images were quantified using NIH ImageJ.

Immunofluorescence analysis (IFA). For immunofluorescence microscopy, BSF or PCF cells were pelleted by centrifugation at 800 × *g* for 10 min at 4°C. Cells were gently resuspended and washed once with ice-cold Voorheis's modified PBS (vPBS) (39). BSF cells were fixed for 10 min and PCF cells for 60 min on ice using 3% paraformaldehyde and vPBS. Excess fixative was washed away, and fixed cells were adhered to poly-lysine-coated slides (Polysine VWR International). For permeabilization, cells were incubated with 0.1% Triton X-100–PBS for 10 min. Cells were blocked for 1 h using 20% FBS–PBS and incubated with primary antibodies diluted in 20% FBS at appropriate dilutions as follows: TbCLH (40) (1:1,000); TbRab5A (41) (1:100); TbRab11, (11) (1:1,000); TbRabX2 (42) (1:200); ISG65 and ISG75 (43) (1:1,000); TbBiP (44) (1:1,000); *T. brucei* transferrin receptor (45) (1:2,000); p67 (46) (1:1,000); HA (Santa Cruz Biotechnology, Inc.) (1:1,000); GFP (Abcam) (1:5,000); FLAG (Sigma-

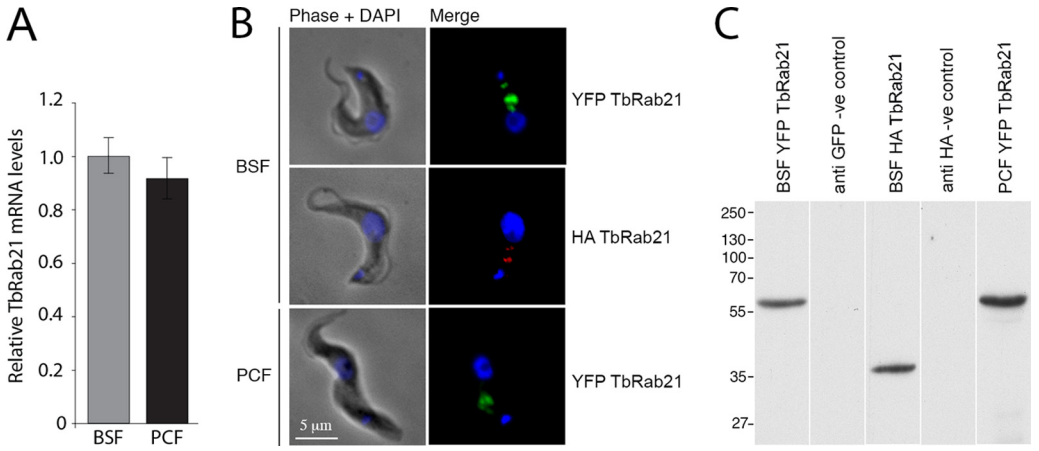

FIG 1 TbRab21 localizes to endocytic regions in trypanosomes. (A) Abundance of TbRab21 mRNA in BSF and PCF cells estimated by qRT-PCR. Data shown represent averages of the results determined for two separate samples normalized to telomerase reverse transcriptase. (B) IFA images showing ectopic expression of TbRab21 fused at its N terminus with yellow fluorescent protein (YFP) or hemagglutinin (HA) tags in BSF cells and YFP in PCF cells. Images were obtained by capturing native YFP- and Alexa Fluor 568-conjugated secondary antibody fluorescence, while DNA was visualized using DAPI staining. (C) Production of the tagged protein verified by Western blot analysis, along with negative (-ve) controls for antibody specificity.

Aldrich) (1:1,000); tubulin KMX-1 (Millipore) (1:500). Secondary antibodies (Oregon green 488 conjugate anti-mouse, Alexa Fluor 488 anti-rabbit, Alexa Fluor 568 anti-mouse, and Alexa Fluor 568 anti-rabbit) were from Invitrogen and used at 1:1,000 dilution. Cells were air dried and coverslips mounted using Vectashield mounting medium with DAPI (4′,6-diamidino-2-phenylindole; Vector Laboratories, Inc.). Cells were observed under a Nikon Eclipse E600 epifluorescence microscope. Images were analyzed using MetaMorph 6.0 software (Universal Imaging Corporation) and figures assembled using Adobe Photoshop (Adobe Systems).

Intracellular trafficking assays. Log-phase cells (5×10^7) were harvested by centrifugation and serum starved for 30 min in serum free HMI-9 1% (wt/vol) bovine serum albumin (BSA). Fluorescein-conjugated concanavalin A (ConA) or Alexa Fluor 633-conjugated human transferrin was added to reach a final concentration of 10 μg/ml or 125 μg/ml, respectively. Cells were incubated at 37°C for different periods of time followed by the addition of ice-cold vPBS to stop uptake. Cells were pelleted, fixed, and mounted as described for the single-cell analyses using a fluorescence microscope or were processed for flow cytometry.

For transferrin recycling, cells were incubated with Alexa Fluor 633-conjugated transferrin as described above. After 60 min of uptake, cells were washed with ice-cold PBS and resuspended in serum-free HMI-9 for different periods. Recycling of transferrin was stopped by chilling cells on ice followed by fixation (20 min using 3% [vol/vol] formaldehyde). Excess fixative was removed with vPBS, and cells were incubated in 3 μM Hoechst 33342 (Invitrogen) solution for 20 min at 37°C. Cells resuspended at 1×10^6/ml were analyzed immediately on a Cyan ADP analyzer (Beckman Coulter, Inc.). Single cells were gated away from clumped cells and further gated according to their cell cycle state using Hoechst 33342 data. Cell-associated fluorescence of 1N1K cells was measured using a 530/40 emission filter for fluorescein and a 665/20 emission filter for Alexa Fluor 633, while these fluorophores were excited using 488-nm- and 635-nm-wavelength lasers, respectively. Hoechst 33342 was excited using a 351-nm-wavelength laser, and data from 50,000 cells of each sample were collected and analyzed using Summit Software (Beckman Coulter).

Protein chemistry. For protein turnover analysis, cycloheximide (Sigma) (100 μg/ml) was added to growing cultures of BSF cells and incubated at 37°C for various periods of time before cell lysate preparation. To separate cytosolic and membrane fractions of total protein, 1×10^8 BSF cells were harvested, washed, and lysed for 5 min on ice using hypotonic lysis buffer (10 mM Tris HCl [pH 7.5]). The lysate was centrifuged at 20,000 × *g* for 10 min at 4°C. The supernatant was removed and mixed with SDS sample buffer. The pellet fraction was resuspended in sample lysis buffer (50 mM Tris HCl [pH 7.5], 150 mM NaCl, and 1% Nonidet P-40) and incubated on ice for 25 min following the addition of SDS sample buffer and heating at 95°C for 10 min. Cell equivalents of cytosolic and membrane fractions were analyzed by SDS-PAGE and Western blotting using TbBiP as a control for the membrane fraction.

Transmission electron microscopy. BSF cells (1×10^8) were harvested by centrifugation and washed with saline (0.1 M HEPES, 0.98% NaCl [pH 7.0]). For ultrastructure analysis, cells were fixed for 4 h on ice using fixative (2% glutaraldehyde, 2 mM $CaCl_2$, 0.1 M PIPES [piperazine-*N*,*N*′-bis(2-ethanesulfonic acid] [pH 7.4]; 100 μl H_2O_2 was added to 10 ml fixative prior to use). After fixation, cells were washed thrice with 0.1 M HEPES (pH 7.0) and the cell pellet was processed further by the University of Cambridge Multi-Imaging Centre. Prepared ultrastructure sections were viewed using a FEI Tecnai G2 transmission electron microscope. Digital images were saved and assembled using Photoshop.

RESULTS

Endosomal Rab21 is expressed in both major life cycle forms of *T. brucei*. To ensure that TbRab21 was expressed, the level of TbRab21 mRNA was estimated by quantitative reverse transcription-PCR (qRT-PCR) in BSF and procycle-form (PCF) cells; similar mRNA levels were observed for the two life stages, and these levels are comparable to those seen with other trypanosome Rab mRNAs, as well as to previous transcriptome data (Fig. 1A) (47, 48).

TbRab21 is expressed in trypanosomes at very low levels, which suggested that either genomic tagging or production of antibodies was unlikely to be informative, in terms of localizing the gene product or estimating protein expression levels. Hence, we used ectopic overexpression of N-terminally tagged TbRab21 via the pHD1034 vector to determine subcellular localization (37). Ectopic TbRab21 was overexpressed at ~10-fold as judged by mRNA levels compared to endogenous expression, at a level that is still extremely low (data not shown). A similar strategy had been used by us previously for TbRab23 and TbRab28 which resulted in no detectable mislocalization compared to that determined with an antibody and is also in common use in studies of mammalian cells for localization of small GTPases and of Rab21 in particular (18, 22, 49). To minimize the possibility that the tag itself resulted

in mislocalization, both 2× HA and YFP-tagged TbRab21 were produced.

Immunofluorescence analysis in BSF cells revealed that HA-tagged TbRab21 was located between the nucleus and kinetoplast, mainly as discrete puncta in interphase cells (Fig. 1B). A similar localization is known for various endomembrane components of *T. brucei* (11, 12, 50), indicating a possible endosomal role for TbRab21. Postmitosis cells, i.e., cells containing two nuclei but prior to cytokinesis, showed a dividing population of TbRab21-positive structures that eventually distributed between the two daughter cells. Analysis also revealed that TbRab21 remained associated with the endomembrane structures throughout the cell cycle, suggesting that trafficking mediated by this protein likely is active during cell division. BSF cells expressing YFP-TbRab21 were fixed and observed for protein localization, avoiding the selective loss of cytosolic proteins in conventional immunofluorescence antibody staining. Additional to the endosomal punctate staining, faint, diffused cytosolic YFP fluorescence, likely corresponding to soluble GDP-bound TbRab21 in complex with Rab-GDI, was observed (Fig. 1B). Thus, similar localization patterns were observed for the YFP-tagged TbRab21 and the HA-tagged TbRab21, which makes the possibility of mistargeting highly unlikely, as this would require HA and YFP tags to mistarget with identical locations, an extremely remote possibility.

PCF cells transfected with a pHD1034:YFP-TbRab21 construct revealed a subcellular localization similar to that of BSF cells. Some PCF cells exhibited TbRab21 puncta anterior to the nucleus, in addition to the puncta located between the nucleus and kinetoplast (Fig. 1B). These anteriorly located puncta of TbRab21 were also very occasionally observed in BSF cells. Anterior staining has also been reported for TbRab5A, but a specific biological role for this Rab population, or what it may represent in terms of endosomal dynamics, has yet to be determined (41, 51). An anterior YFP-TbRab21 punctum in some PCF cells was also found at the anterior tip of the cell body but was apparently not related to any particular phase of the cell cycle. Finally, Western blotting of BSF and PCF lysates from cells expressing tagged TbRab21 confirmed the in-frame production of correctly sized proteins (TbRab21, 28 kDa; YFP-TbRab21, 55 kDa), with no apparent degradation products observed (Fig. 1C).

Rab GTPases cycle between an inactive cytosolic pool and an active membrane-associated pool. To assess the distribution of overexpressing tagged TbRab21s in BSF cells, particulate and soluble fractions were prepared by hypotonic lysis and Western blotting was performed. TbBiP, an ER lumenal protein, was used as a loading control and was found predominantly in the membrane fraction as expected, while HA-tagged TbRab21 was ~60% cytosolic and ~40% membrane bound, consistent with the immunofluorescence results determined for YFP-TbRab21 (Fig. 1B). The efficiency of lysis was further confirmed by the total protein staining of supernatant and pellet fractions (see Fig. S1A in the supplemental material). These data also further support the hypothesis of correct targeting, as the proportion of membrane-bound TbRab21 is similar to that of endogenous Rab proteins (see, e.g., reference 52). Turnover of HA-tagged TbRab21 was also analyzed in BSF cells where protein synthesis had been blocked with cycloheximide, and the residual levels of HA-TbRab21 were quantified by Western blotting. Based on these data, HA-tagged TbRab21 has a half-life of ~7 h (Fig. S1B). To ensure complete blocking of protein synthesis after cycloheximide treatment, lysates from treated cells were also assessed for the half-life of additional known proteins; ISG65 and ISG75 had turnover kinetics similar to previously reported observations (data not shown) (50). Hence, TbRab21 has a turnover time that is similar to that of the cell cycle.

Subcellular localization of TbRab21. To determine the spatial relationship of TbRab21 with other markers of the *T. brucei* endomembrane system, immunofluorescence experiments were performed. Endocytosis in *T. brucei* is exclusively clathrin mediated, and clathrin is known to be distributed throughout the endocytic and *trans*-Golgi regions of the cell (2). IFA demonstrated that HA-tagged TbRab21 partially overlapped with clathrin heavy-chain staining (88%) and is consistent with the diverse endosome and Golgi membrane localizations of clathrin (Fig. 2A; see also Table S1 in the supplemental material).

HA-tagged TbRab21 also exhibited partial overlap with TbRab5A (83%), a marker for early endosomes (Fig. 2A; see also Table S1 in the supplemental material). Human Rab21 colocalizes with Rab5A on early endosomes (22), but in *T. brucei*, the partial overlap revealed even by less-discriminating wide-field microscopy suggests that TbRab21 function is not restricted to Rab5 early endosomes. TbRab21 was also found juxtaposed to the recycling/exocytic TbRab11 in BSF cells. As expected, TbRab11 was observed closer to the flagellar pocket whereas HA-TbRab21 was deeper toward the nucleus. TbRab21 was clearly distinct from TbRab11-labeled recycling endosomes in some cells (56%), while there was some (44%) overlap in others due to close proximity of the early and recycling structures in *T. brucei*. TbRabX2 (formerly TbRab31) was used as a marker for Golgi complex (53). IFA showed that HA-TbRab21 was distinct from TbRabX2 and therefore had no obvious steady-state presence on the Golgi complex (Fig. 2A). To elucidate the location of TbRab21 with reference to late endosomes and the vacuole/lysosome, p67 was chosen as a marker. p67, a LAMP-like *trans*-membrane lysosomal glycoprotein (54), was found juxtaposed to tagged TbRab21, but little (15%) overlap was observed. The partial overlap of TbRab21 with early endosomes and juxtaposition to the lysosome suggested a possible localization to intermediate endocytic structures. To explore this possibility, TbVps23 (an orthologue of mammalian TSG101) was used as a marker for the intermediate or late endosome/multivesicular body (MVB). TbVps23 is a member of ESCRT-I (endosomal sorting complex required for transport-I) and is required for the recognition and sorting of ubiquitinated cargo (50). Immunofluorescence of YFP-TbRab21 and HA-TbVps23 revealed partial (70%) colocalization.

We have previously observed colocalization between TbVps23 and a second trypanosome Rab, TbRab28. As this protein appears to coordinate retromer-dependent and ESCRT-mediated pathways (18), we assessed whether there was an overlap in the TbRab21 and TbRab28 localizations. Coexpression of HA-TbRab28 and YFP-TbRab21 revealed a good degree (79%) of colocalization, although not complete colocalization, suggesting that these two Rabs are targeted to similar, but nonidentical, endosomal membrane microdomains. Taking these data together, we conclude that TbRab21 in BSF cells is present on both early and intermediate/late endosomes. In PCF cells, where endocytic structures are less well developed, YFP-tagged TbRab21 showed predominant (85%) colocalization with TbRab5A (Fig. 2A; see also Table S1 in the supplemental material).

To confirm a functional role for TbRab21 on endosomes, colocalization with cargo molecules was analyzed. Concanavalin A

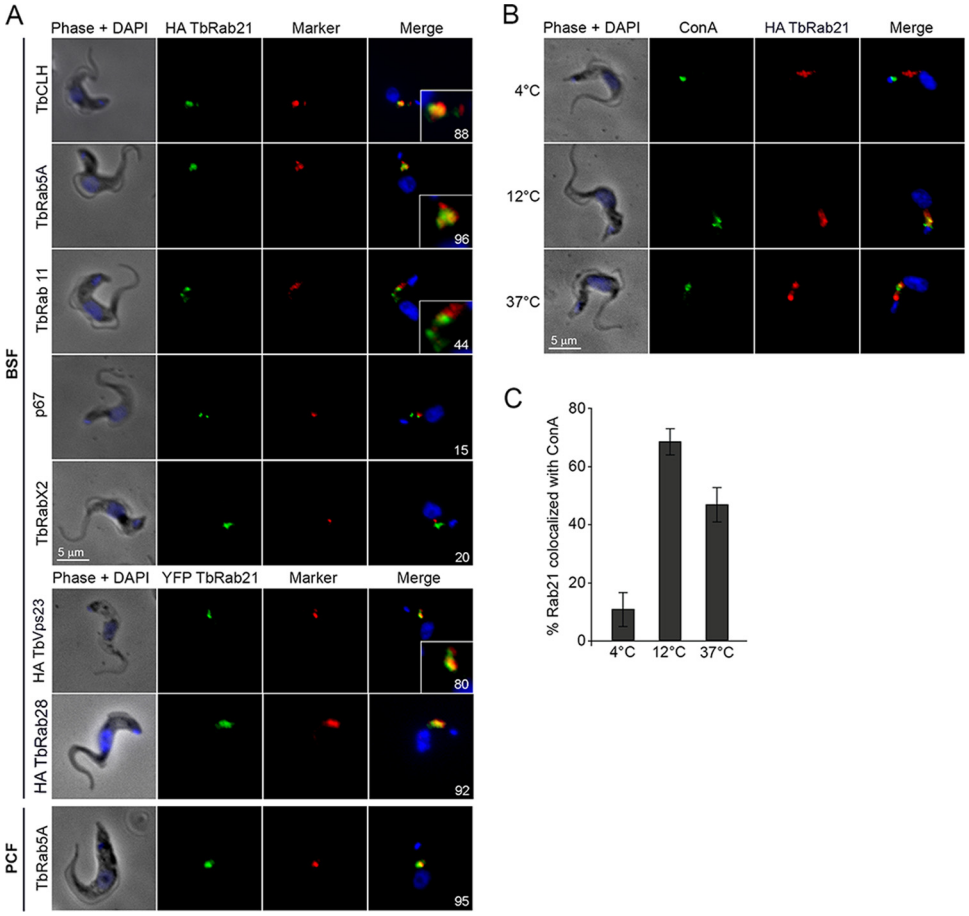

FIG 2 TbRab21 defines a new endosomal subcompartment. (A) BSF and PCF cells stably expressing TbRab21 tagged with N-terminal HA or YFP were costained with markers of the *T. brucei* endomembrane system. Cells were labeled with mouse monoclonal antibodies against the HA epitope tag in addition to antibodies against *T. brucei* clathrin heavy chain (TbCLH), TbRab5A, TbRab11, p67, and TbRabX2. For costaining with TbVps23 and TbRab28, BSF cells expressing YFP-TbRab21 were transfected with HA-TbVps23 and HA-TbRab28. Alexa Fluor-labeled secondary antibodies and YFP native fluorescence were used to visualize subcellular markers, while nuclear and kinetoplast DNA was visualized using DAPI. Percent colocalization is shown at the bottom right of each set of panels; see Table S1 in the supplemental material for complete data. (B) BSF cells expressing HA-tagged TbRab21 were subjected to a continuous pulse of fluorescein-conjugated ConA at 4, 12, and 37°C. (C) HA-TbRab21 fluorescence intensity colocalization with ConA. A total of 25 randomly selected cells from each sample were analyzed and the percentages of colocalization determined.

(ConA), a mannose-binding lectin which binds VSG, was incubated with BSF cells expressing HA-tagged TbRab21. ConA taken up by cells is transferred from early to late endosomes and ultimately accumulates in the lysosome. When incubations are performed at different temperatures, ConA labels various endocytic structures. At 4°C, ConA was restricted to the flagellar pocket (FP) and HA-TbRab21 was not colocalized, suggesting that TbRab21 is unlikely to act at the FP membrane (Fig. 2B). At 4°C, a low level (10.5% ± 5.8% standard error) of TbRab21 colocalized with ConA, which was most likely due to the technical difficulty of maintaining ConA in the FP, as processing can allow cells to warm above 4°C, resulting in some ConA progression to early endosomes. At 12°C, ConA was blocked at the early endosome and TbRab21 and ConA showed significant colocalization (68.1% ± 4.5%). At 37°C, when some of the ConA had reached the lysosome, and due to the continuous uptake also labeling early and late endosomes, the level of TbRab21 colocalized with ConA was reduced to 46.5% ± 5.9% (Fig. 2C). These data indicate that the TbRab21-positive compartment is capable of receiving endocytic cargo.

TbRab21 is essential for proliferation of bloodstream-form cells. To assess the importance of TbRab21 for normal proliferation of BSF cells and to investigate possible functions, knockdown of TbRab21 expression was achieved by RNA interference. Induction of double-stranded RNA (dsRNA) against TbRab21 resulted in a severe growth defect (Fig. 3A). The impact on proliferation was reproducibly observed in multiple transfections and RNAi clones. The effect of RNAi on proliferative capacity was observed very rapidly; cells underwent one cell cycle and proliferated slowly afterwards, and a recognizable phenotype could be seen as early as 12 h postinduction, suggesting that this resulted directly from loss of TbRab21 and was not due to secondary effects. Efficiency and specificity of RNAi were assessed by qRT-PCR. Results obtained from duplicate inductions showed a 50% reduction in TbRab21 mRNA levels after 24 h of induction (Fig. 3B). To determine the effect of RNAi on protein levels, HA-tagged TbRab21 was expressed in TbRab21 RNAi cells. Western blotting showed specific loss of tagged TbRab21 that was reduced to less than 5% after 24 h of RNAi induction (Fig. 3C). These data therefore confirm the

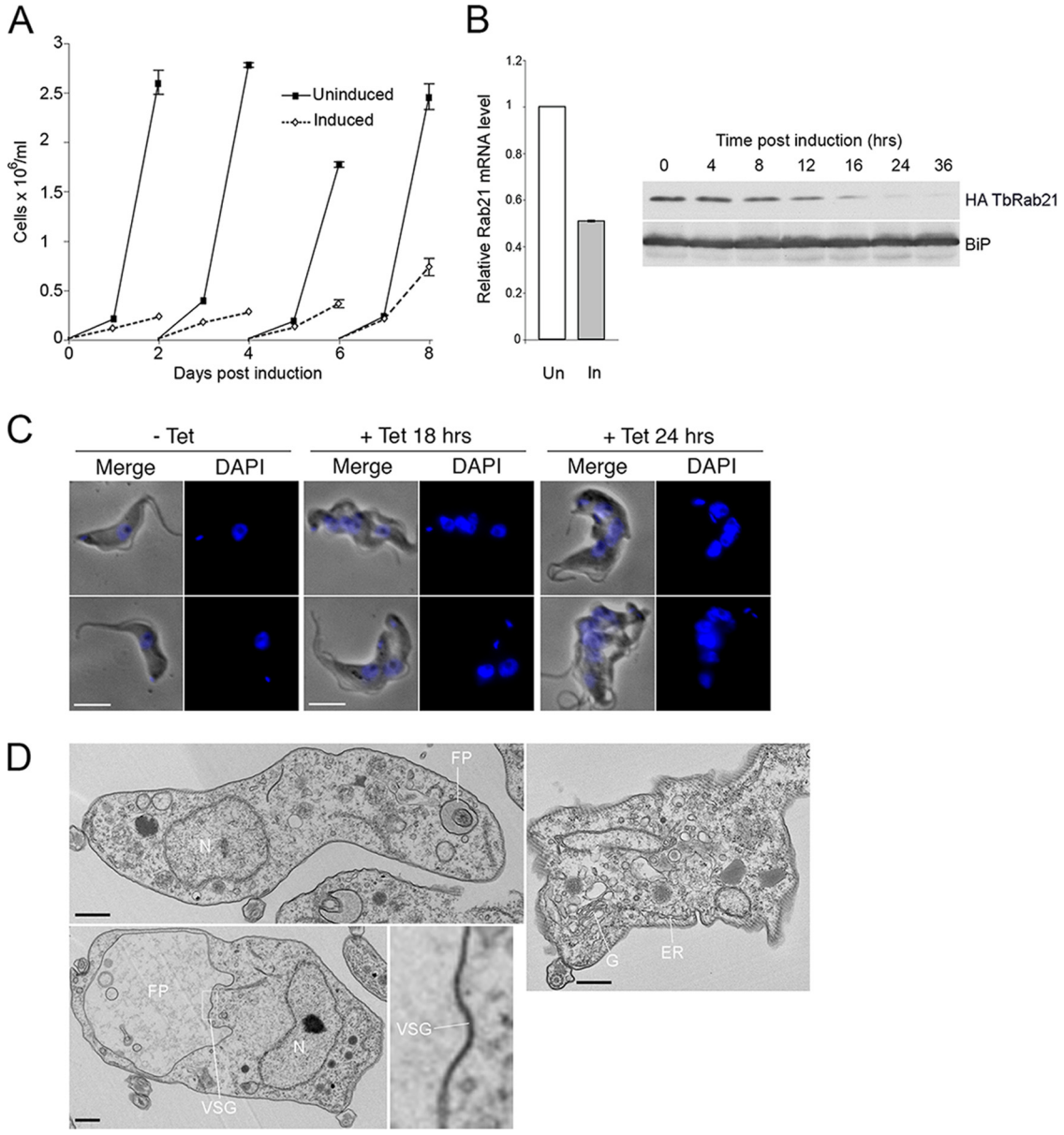

FIG 3 TbRab21 is required for correct cell cycle progression but does not affect flagellar pocket morphology. (A) Growth curve of BSF TbRab21 knockdown cells. RNAi cells were grown in the presence (broken lines) or absence (solid lines) of 1 μg/ml tetracycline (Tet) to induce transcription of dsRNA. Cell numbers were determined every 48 h (error bars represent the standard errors of duplicate inductions). (B) Validation of TbRab21 RNAi by qRT-PCR and Western blotting. (Left) RNA was extracted from uninduced and 24-h-induced cultures in duplicate, and qRT-PCR was performed in triplicate for each sample. (Right) Validation of knockdown by Western blotting. Copy numbers of overexpressed HA-tagged TbRab21 decreased specifically after the induction of TbRab21 RNAi. TbBiP is shown as a loading control. (C) Phase and DAPI images of cells at 18 and 24 h of induction. An uninduced (-Tet) cell is shown for comparison to the variation observed in induced cells (+Tet), with clear signs of failed cytokinesis. All images were captured at the same magnification. Bar, 5 μm. (D) Ultrastructure of TbRab21 knockdown BSF cells. (Clockwise from top left) Cells 12 h postinduction with normal flagellar pocket (FP) and nucleus (N); 18-h-induced cell showing normal morphology of Golgi complex (G) with *cis*- and *trans*-faces, ER exit site, and normal morphology of endoplasmic reticulum (ER); and cell 12 h postinduction showing an enlarged flagellar pocket (BigEye phenotype); a distinctive electron dense VSG layer (VSG) can be seen around the enlarged pocket. An inset of the FP membrane showing the electron-dense VSG coat is shown at center. Images were captured at various magnifications; all scale bars denote 500 nm.

specificity of the knockdown as well as demonstrate that the kinetics of protein and mRNA suppression and normal proliferation are consistent with each other, suggesting that these events are directly connected.

To elucidate the precise nature of the defect, cells harboring the TbRab21 knockdown construct were induced and analyzed for the numbers of nuclei and kinetoplasts by DAPI staining (see Fig. S2 in the supplemental material). A gradual accumulation of cells with more than two nuclei and two kinetoplasts was observed, which suggests a failure in cytokinesis, but with continued nuclear and kinetoplast replication, while the proportion of cells with a single nucleus and kinetoplast, i.e., G_1 cells, was reduced accordingly. Examples of "monster" cells, i.e., with multiple nuclei and kinetoplasts, are shown in Fig. 3C. These may have arisen as a

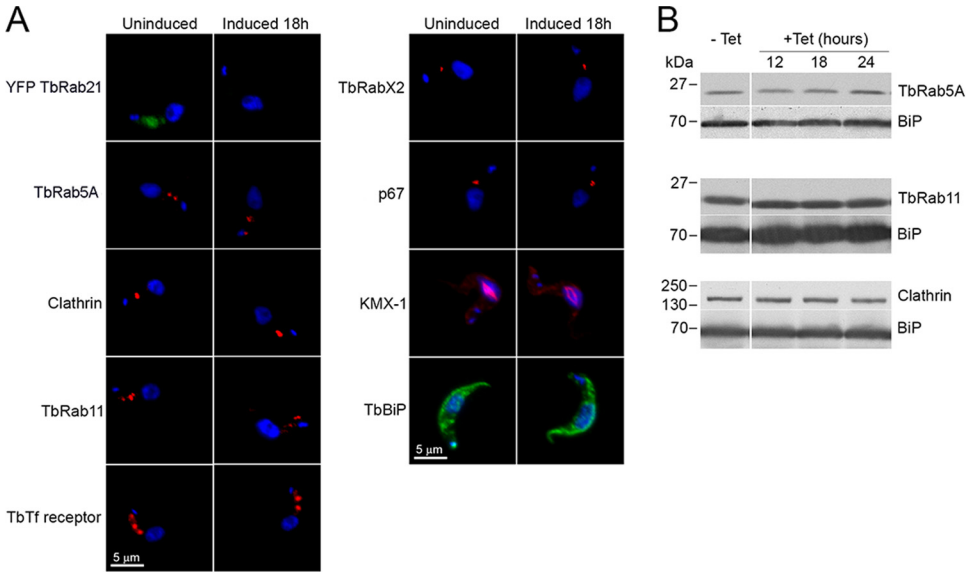

FIG 4 The morphology of most endomembrane compartments is not critically dependent on TbRab21 expression. (A) Immunofluorescence analysis of *T. brucei* endosomal components performed on TbRab21-depleted BSF cells. (B) Total protein levels of TbRab5A, TbRab11, and TbClathrin were quantified by Western blotting in TbRab21-depleted cells. The BSF RNAi TbRab21 cell line was induced and cell lysate prepared at different time intervals. TbBiP was used as the total protein loading control.

consequence of secondary effects due to TbRab21 knockdown, with proteins being mislocalized and thus resulting in a "traffic jam" that ultimately affected the completion of cytokinesis. To exclude the possibility of selective attachment of cells with polylysine slides, induced and uninduced cells were also analyzed by flow cytometry, and these data were consistent with DAPI analysis, i.e., an increase in postmitotic cells with tetraploid (4n) DNA content (data not shown). Enlargement of the flagellar pocket, which frequently occurs after depletion of proteins involved in early steps of endocytosis, including TbRab5A and clathrin (2, 13), was observed in only 5% of TbRab21-depleted cells; this rather low frequency of the BigEye morphology suggests that the phenotype is secondary in nature and therefore that TbRab21 is not significantly involved in early endocytosis. Based on the severity of the proliferative defect and the possibility of the emergence of secondary defects, the time 18 h postinduction was selected for analysis of TbRab21 knockdown cells in subsequent experiments.

To further explore the nature of any morphological defects in subcellular compartments resulting from TbRab21 knockdown, thin sections of induced RNAi BSF cells were observed by transmission electron microscopy. Cells from two different time points, 12 and 18 h postinduction, were analyzed together with uninduced cells. Results based on approximately 30 randomly selected cells from each sample had a normal morphology of most membrane trafficking compartments and other subcellular structures (Fig. 3D). Approximately 5% of the cells from both 12 and 18 h postinduction showed massively swollen flagellar pockets, and the proportion of BigEye cells was therefore consistent with that observed by light microscopy. The Golgi complex appeared normal even in 18-h-induced cells, distinct from a TbRab28 knockdown where the Golgi complex disintegrates (18). Therefore, these data indicate that TbRab21 has functions that are restricted to the endocytic system and do not, at least as shown in this analysis, impact on additional cellular systems or have a profound impact on the very earliest steps in endocytosis from the flagellar pocket.

Analysis of subcellular markers in TbRab21-depleted cells. Before analyzing the effects of TbRab21 knockdown on subcellular markers, depletion of TbRab21 was ensured in individual cells by overexpressing YFP-tagged TbRab21 in TbRab21 knockdown cells and inducing RNAi. Single-cell analysis of YFP native fluorescence by microscopy revealed complete loss of TbRab21 from all of the 18-h-induced cells, including the normal-morphology 1N1K cells (Fig. 4A). Induced and uninduced cultures were grown to reach comparable cell densities as ectopic expression from ribosomal promoters is density dependent in BSF cells (55). In the subsequent analysis of TbRab21 knockdown, IFA included only cells with normal morphology to avoid major artifacts due to disruption of structures resulting from secondary effects, whereas Western blotting of total protein from whole-cell lysates represented the entire cell population.

Rab21 is evolutionarily related to Rab5 (21), and whereas the knockdown of TbRab5A or TbRab5B results in a decrease of clathrin protein copy numbers (13), Western blotting indicated that clathrin protein levels remained unchanged following induction of RNAi against TbRab21 (Fig. 4B). Similar results were obtained by immunofluorescence, where the fluorescence levels and locations of clathrin were similar in uninduced and 18-h-postinduction cells (Fig. 4A). These data suggest that TbRab21 does not function at the early steps of endocytosis, consistent with the absence of BigEye cells in significant proportions upon induction. Similarly, TbRab5A protein levels remained unchanged when TbRab21 was depleted, and the endosomal localization of TbRab5A was unperturbed. These data suggest that TbRab5A is independent of TbRab21 in terms of membrane localization and possibly acts upstream of TbRab21. A modest increase in the total amount of TbRab5A was observed by Western blotting; this could have been a compensation for loss of TbRab21, but the effect was

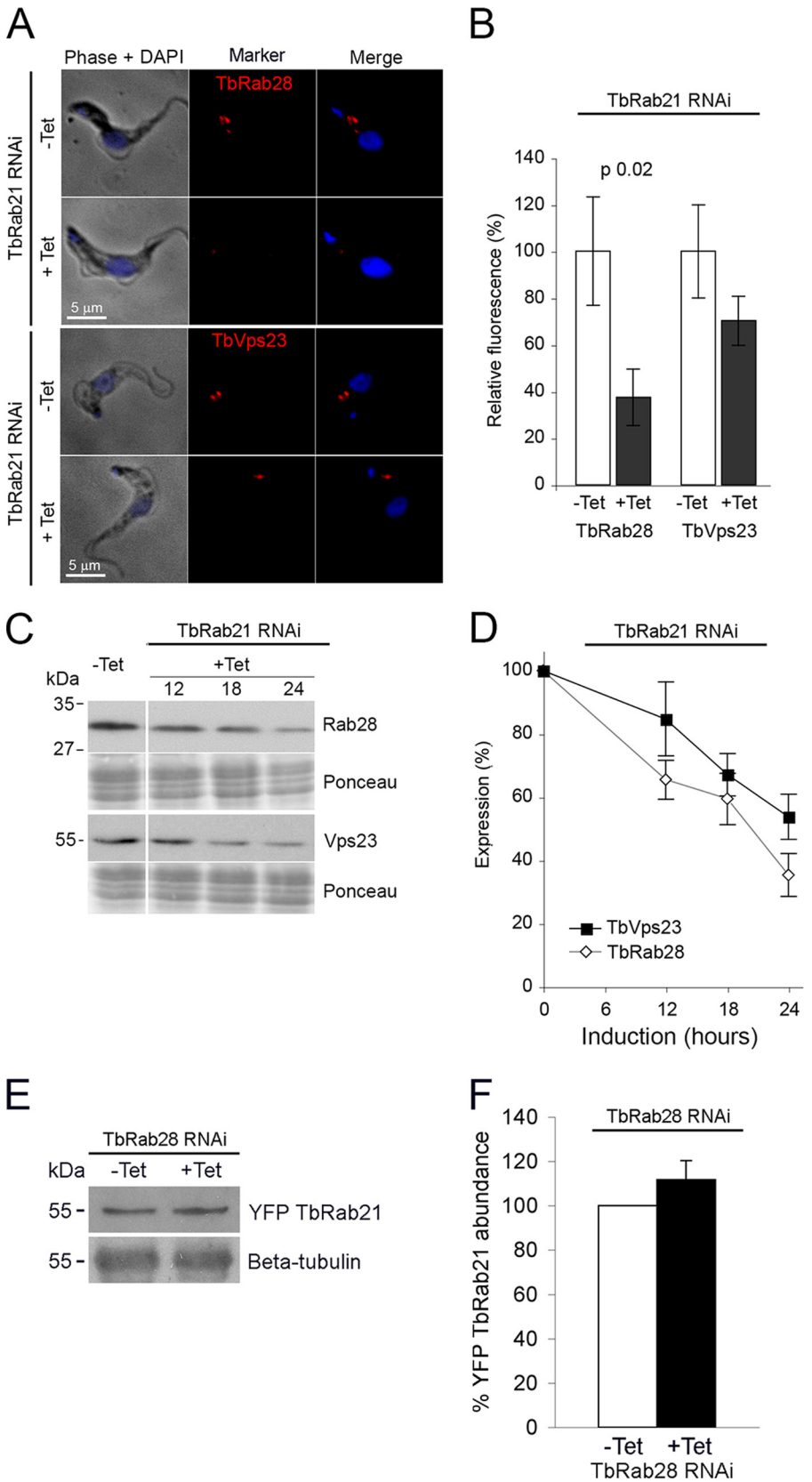

FIG 5 TbRab21 is required for maintaining expression of intermediate endosomal components. (A) Immunofluorescence analysis of HA-tagged TbRab28 and TbVps23 in TbRab21 knockdown cells. −Tet (uninduced control) and +Tet (18 h induced) cells were fixed and stained for the HA epitope tag using mouse anti-HA and Alexa Fluor 568 (red) antibodies, while DNA was counterstained using DAPI (blue). Images were captured under identical exposure conditions, and

quite minor. No effect was observed on the copy number or localization of TbRab11 after TbRab21 silencing by IFA and Western analysis (Fig. 4), suggesting that the recycling pathway is unperturbed.

The *T. brucei* transferrin receptor (ESAG6 and -7 [ESAG6/7]) is a glycosylphosphatidylinositol (GPI)-anchored molecule that recycles between endosomes and the flagellar pocket and is responsible for the uptake of iron-laden transferrin (reviewed in reference 56). The intracellular localization and total protein levels of the transferrin receptor (TfR) were analyzed in TbRab21 knockdown BSF cells. As expected, immunofluorescence observations revealed no obvious difference in the localization pattern of TfR following RNAi, a further indication that TbRab21 is not directly involved in recycling or early steps of endocytosis in comparison to TbRab11 RNAi, which relocates TfR from the flagellar pocket to intracellular regions of the cell, and clathrin RNAi, which restricts TfR to the flagellar pocket (2, 58). Knockdown of TbRab21 resulted in an approximately 40% increase in the total amount of TfR as quantified by Western blotting (see Fig. S3 in the supplemental material). BSF cells are known to upregulate TfR expression to compensate for reduced availability of iron (58), which may suggest a role for TbRab21 in iron uptake and suggest an impact on iron uptake that is distinct from the trafficking of the TfR and possibly in later events where transferrin is degraded and iron realized in later endosomal compartments.

Lysosomal morphology appeared unaffected as no significant alterations in the localization of p67 were observed by immunofluorescence after induction of RNAi against TbRab21 (Fig. 4A). Similarly, the morphology of the Golgi complex, as revealed by TbRabX2 observations, was unperturbed in TbRab21-depleted BSF cells, consistent with the ultrastructural data. The normal Golgi morphology suggests that TbRab21 does not play a direct role in regulation of retrograde transport from the endosome to the Golgi pathway. These results distinguish TbRab21 from late endosomal TbRab28, where evidence suggests a participation in retrograde trafficking, due to the TbRab28 knockdown leading to the gradual fragmentation of Golgi membranes (18).

TbRab21 knockdown results in loss of MVB/late endosomal components. TbRab21 knockdown resulted in a reduction in the steady-state levels of both TbRab28 and TbVps23 as analyzed by immunofluorescence and Western blotting which was very reproducible (Fig. 5). TbRab28 is a late endosomal protein that likely functions upstream of the ESCRT-I component TbVps23 (18). In the absence of antibodies, HA-tagged TbRab28 and TbVps23 were independently expressed in TbRab21 RNAi BSF cells. The decrease in the TbRab28 copy number preceded TbVps23 loss and was also greater in magnitude; this is consistent with previous work where TbRab28 silencing led to a very significant decrease in TbVps23 levels (18). In contrast, RNAi-mediated depletion of TbRab28 had no obvious effect on TbRab21 steady-state levels (Fig. 5E and F), suggesting that TbRab21 functions upstream of TbRab28, while RNAi-mediated depletion of TbRab28 in turn resulted in a decrease in TbVps23 levels.

Due to the cell density-dependent nature of ectopic expression, analysis was performed to account for the reduced expression at higher culture densities by normalizing induced culture results to the level of expression in uninduced cultures at a similar cell density (55). This secondary effect on the TbRab28 protein level further limits the possibility of studying defects caused by the loss of TbRab21, as depletion of TbRab28 by RNAi knockdown causes a multitude of endocytic defects, including perturbed lysosomal delivery of ubiquitinated cargo and retromer-dependent trafficking (18).

The possibility that defects observed after TbRab21 depletion result from a secondary loss of TbRab28 can be most likely excluded as the cell cycle defects observed after the knockdown of TbRab21 appeared quickly and before significant reduction in TbRab28 expression. Also, the phenotypes were highly distinct from each other, with no cell cycle defect observed for TbRab28 RNAi (18) and no Golgi disintegration after TbRab21 depletion. A similar argument can also be applied to TbVps23, where direct suppression by RNAi did not cause a block to cell cycle progression (50). Therefore, these data suggest a synthetic interaction between TbRab21, TbRab28, and TbVps23.

TbRab21 is required for the transport of cargo from endosomes to the lysosome. To elucidate the role of TbRab21 in regulating late endocytic events, particularly the transport of ubiquitinated cargo, the fates of invariant surface glycoprotein 65 (ISG65) and ISG75 were analyzed in TbRab21-depleted BSF cells. ISGs are high-abundance *trans*-membrane domain surface proteins in trypanosomes that are internalized by a ubiquitin- and ESCRT-dependent mechanism (53, 57).

The internal pools of ISG65 and ISG75 were analyzed after 18 h of induction of RNAi against TbRab21 by staining for internal antigen by immunofluorescence using polyclonal antibodies to both proteins. Data from these single-cell analyses showed a significant and reproducible increase in the fluorescence signals obtained with antibody to ISG65 and ISG75 and associated with endosomal structures, whereas, by contrast, the total level of these proteins, as quantified by Western blotting and densitometry, remained unchanged (Fig. 6). This increased level of internal ISG suggests a block in the movement of cargo into the degradative endosomal pathway and hence decreased turnover. The increase in the amount in the internal pool with total ISG remaining unchanged also suggested a corresponding decrease in the amount of the surface fraction, but despite repeated attempts by IFA and flow cytometry, no such reduction was observed (data not shown); this is likely an access problem, with the superabundant VSG occluding many epitopes and hence compromising quantitative analysis,

a reduction in the intensity of HA-TbRab28 and HA-TbVps23 associated with endosomes was observed after induction of RNAi against TbRab21. (B) Quantification of HA-TbRab28 and HA-TbVps23 fluorescence in cells from panel A. A total of 40 randomly selected cells from each sample were analyzed under nonsaturating conditions using Metamorph software. Results for induced cultures were normalized to uninduced controls set to 100%. Error bars represent standard errors of the means. (C and D) Following knockdown of TbRab21, total protein levels of HA-TbRab28 and HA-TbVps23 were quantified by Western blotting. Proteins were quantified using ImageJ by normalizing individual lanes to Ponceau S total protein loading controls. The average numbers of multiple inductions ($n = 3$ to 5) were plotted normalized to uninduced cells normalized to 100%. Error bars show standard errors of the means. (E and F) RNAi-mediated knockdown of TbRab28 was induced for 36 h followed by Western blotting to monitor levels of YFP TbRab21. Beta-tubulin was used as a loading control. Results for induced cultures were normalized to uninduced controls (100%). Error bars represent standard errors of the means. For each panel, the relevant RNAi target is shown above a bar.

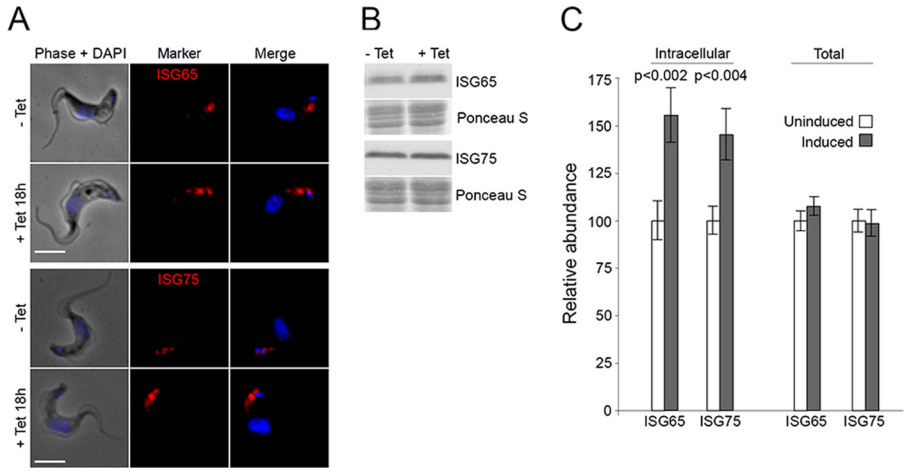

FIG 6 TbRab21 is involved in surface protein turnover. (A) IFA of ISG65 and ISG75 in TbRab21 RNAi cells. −Tet (uninduced control) and 18 h +Tet (induced) cells were fixed and treated with 0.1% Triton X-100 to permeabilize cells and remove most of the surface ISGs. The internal, endosomal ISG pool was stained using polyclonal anti-ISG65 and ISG75 antibodies that were visualized using Alexa Fluor 568-labeled secondary antibodies. Images were captured under identical exposure conditions. Bar, 5 μm. (B) Total levels of ISG65 and ISG75 was quantified by Western blotting, following knockdown of TbRab21. (C) Levels of endosomal ISG65 and ISG75 were quantified in TbRab21 RNAi cells by IFA. A total of 30 randomly selected induced (18 h) and uninduced cells were analyzed under nonsaturating conditions using Metamorph software. Results showed significant increases in the endosomal pools of ISGs after TbRab21 depletion, whereas total ISG levels remained unchanged.

and has been observed by us for ISG surface quantitation on several occasions (K.F.L. and M.C.F., unpublished observations).

A similar increase in the internal ISG pool has also been observed following knockdown of late endocytic proteins, including TbRab28 (18), while knockdown of proteins functioning in the early steps of endocytosis, e.g., clathrin and TbEpsinR, leads to a reduction in the internal pool of ISGs (72). To investigate the effect of the apparent block of ISGs on their lysosomal degradation, TbRab21 knockdown and control cells were incubated with cycloheximide and the level of residual ISG at various time points was quantified by Western blotting. Densitometry demonstrated a modest decrease in ISG turnover, and ~10% more ISG65 and ISG75 was detected in TbRab21 knockdown cells than in uninduced cells after 6 h of cycloheximide treatment (data not shown). This may reflect the highly active trypanosome endocytic pathway and incomplete suppression of TbRab21, although this was quite efficient, as shown in Fig. 3. Alternatively, and more probably, this may indicate the presence of distinct pathways unaffected by TbRab21 and recalls the incomplete block to degradation obtained by knockdown of TbVps23 (50, 59). Such a low level of protection indicates that the vast majority of ISG65 and ISG75 degradation was unperturbed by TbRab21 knockdown.

The role of TbRab21 in uptake and recycling. To explore the role of TbRab21 in endocytic ligand uptake and recycling, assays were performed using fluorophore-labeled ConA and transferrin. Uptake was assayed by incubating TbRab21-depleted and control cells with fluorescein-conjugated ConA for various times and determining the accumulated fluorescence by flow cytometry. No difference in uptake between uninduced and induced TbRab21 RNAi cells was observed (Fig. 7A), whereas a control uptake assay using TbRab5A RNAi BSF cells showed significantly reduced uptake in induced cells compared to the uninduced population (data not shown). These results indicated once more that TbRab21 is not involved in the early steps of endocytosis. Only interphase 1N1K cells were included in the analysis, excluding the TbRab21-depleted 2N2K or >2N2K cells. This introduced an apparent bias in the analysis by excluding highly defective cells, but the cytokinesis defect resulted in multiple copies of the endocytic apparatus, nonspecific binding, and likely other defects and hence apparent greater ConA accumulation but could have been due to multiple factors. Further, monster cells bind ConA nonspecifically at the surface, presumably due to gross disruption of membrane structure. However, similar results were obtained when cells were analyzed by microscopy and ConA fluorescence was manually quantified using Metamorph software (data not shown).

As TbRab21-depleted cells are able to take up and accumulate ConA in endocytic structures, their ability to transfer lectin to the lysosome was analyzed by calculating colocalization of intracellular ConA with the p67 lysosomal marker. This analysis detected a small but significant decrease in the amount of ConA reaching the lysosome in TbRab21-depleted cells (Fig. 7B and C). This modest block to lysosomal transport is consistent with the presence of increased internal pools of ISGs. Taken together, these data suggest that loss of TbRab21 causes a partial prelysosomal block in endosomal traffic.

To assess receptor-mediated endocytosis and recycling in TbRab21 RNAi cells, Alexa Fluor 633-labeled transferrin was used. BSF cells take up transferrin from the serum of their host, and a trypanosome-specific transferrin receptor delivers surface transferrin to the endosomes. The transferrin receptor is recycled to the pocket approximately 60 times before degradation, while transferrin is degraded in the lysosome, from which location it is exported as peptides via a recycling pathway (12, 60). Transferrin uptake was followed by incubating uninduced and induced TbRab21 RNAi cells with fluorophore-conjugated transferrin and quantifying fluorescence by microscopy and flow cytometry. No difference in kinetics or total uptake was observed between TbRab21-depleted and control cells (see Fig. S3A in the supplemental material).

The recycling ability of TbRab21 RNAi cells was assessed by incubating cells with fluorophore-labeled transferrin for 1 h, after which cells were transferred to fresh medium and the quantity of

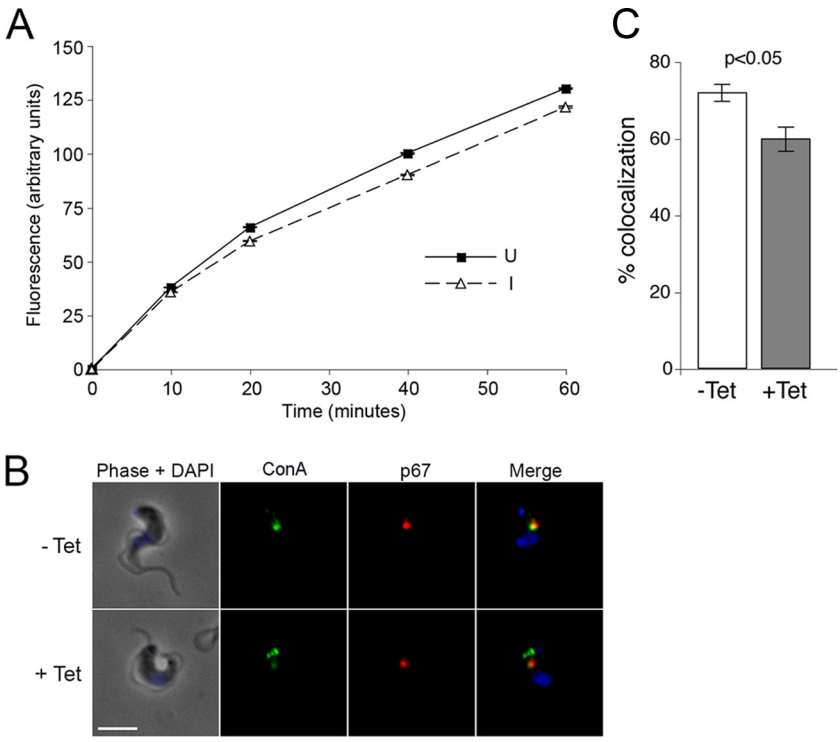

FIG 7 TbRab21 is required for normal concanavalin A trafficking to the lysosome. (A) Endocytic ability of BSF TbRab21 RNAi cells was analyzed by incubating induced (I) and uninduced (UI) cells with fluorescein-conjugated ConA at 37°C. The uptake of ConA was analyzed on a Cyan ADP fluorescence-activated cell sorter (FACS) analyzer. Only 1N1K cells were included in the analysis (gating based on Hoechst staining). Approximately 50,000 cells were counted for each sample, and the median fluorescence of ConA was plotted against time of uptake, with error bars showing standard errors of the medians. Results from a representative of multiple independent inductions are shown. (B) IFA images of BSF TbRab21 RNAi cells showing localization of ConA and lysosomal marker p67. Uninduced (-Tet) and 18 h induced (+Tet) cells received a 15-min continuous pulse of fluorescein-conjugated ConA (green) at 37°C. Cells were fixed and costained with mouse anti-p67. (C) The percentages of ConA fluorescence intensity colocalized with p67 fluorescence were calculated using an ImageJ plug-in for colocalization analysis. A total of 30 randomly selected cells (excluding those morphologically defective) from each sample of induced and uninduced cells were subjected to analysis, and percent colocalization was plotted, with error bars representing standard errors of the means. The experiment was repeated on two independent inductions, and Student's *t* test showed a statistically significant difference between induced and uninduced cells for each induction.

remaining fluorescence was determined at various time points. TbRab21-depleted cells were marginally slower in exporting transferrin fragments through the recycling pathway, while the kinetics of recycling were similar to those of control uninduced cells (see Fig. S3B in the supplemental material). Further, the transferrin receptor expression level appears to be sensitive to the ability of the parasite to accumulate iron, and measurement of the level of the ESAG6 and -7 proteins in induced cells detected only a small increase in the protein copy number, suggesting that the cells were not experiencing a major defect in iron accumulation (see Fig. S3C in the supplemental material). Overall, these data indicate only a very minor impact of TbRab21 suppression on the uptake of transferrin.

Membrane recruitment of TbRab21 is independent of TbRab5A but depends on TbVps23. Our data suggest that TbRab21 functions at late endosomes, upstream of TbRab28, while partially overlapping by location with early endosomal TbRab5A. To elucidate the relationship between TbRab21 and TbRab5A, immunofluorescence and Western analyses were performed on BSF cells overexpressing HA-tagged TbRab21 in a TbRab5A knockdown background. TbRab21 maintained membrane localization after 36 h of TbRab5A suppression, even in BigEye cells, and no apparent difference in the punctate staining of TbRab21 was observed (Fig. 8A). The total protein level of TbRab21 also remained unperturbed, despite TbRab5A becoming barely detectable after 12 h of induction (Fig. 8B, upper panel). These data suggest that TbRab5A knockdown does not affect membrane recruitment or copy numbers of TbRab21.

Surprisingly, the loss of clathrin that occurs following TbRab5A depletion (13) was not observed when such cells were also overexpressing TbRab21 (Fig. 8B, lower panel). To explore the possibility that TbRab21 overexpression synthetically suppressed the effects of TbRab5A knockdown, proliferation of TbRab5A-depleted and proliferation of TbRab5A-depleted/TbRab21-overexpressing cells were compared, but no difference was observed (data not shown). To analyze the effects of TbRab5A knockdown on the intracellular pool of ISG75, induced and uninduced cells were permeabilized and stained for the internal pools of ISG75. Roughly 4-fold-lower levels of internal ISG75 were seen in the TbRab5A-depleted cells, consistent with knockdown of early endosomal proteins causing a reduction of internalized ISG abundance (Fig. 8C and D).

To confirm a relationship between ESCRT component TbVps23 and TbRab21, a BSF RNAi cell line inducible for TbVps23 knockdown was transfected with HA-tagged TbRab21. Induced cells were analyzed by immunofluorescence and Western

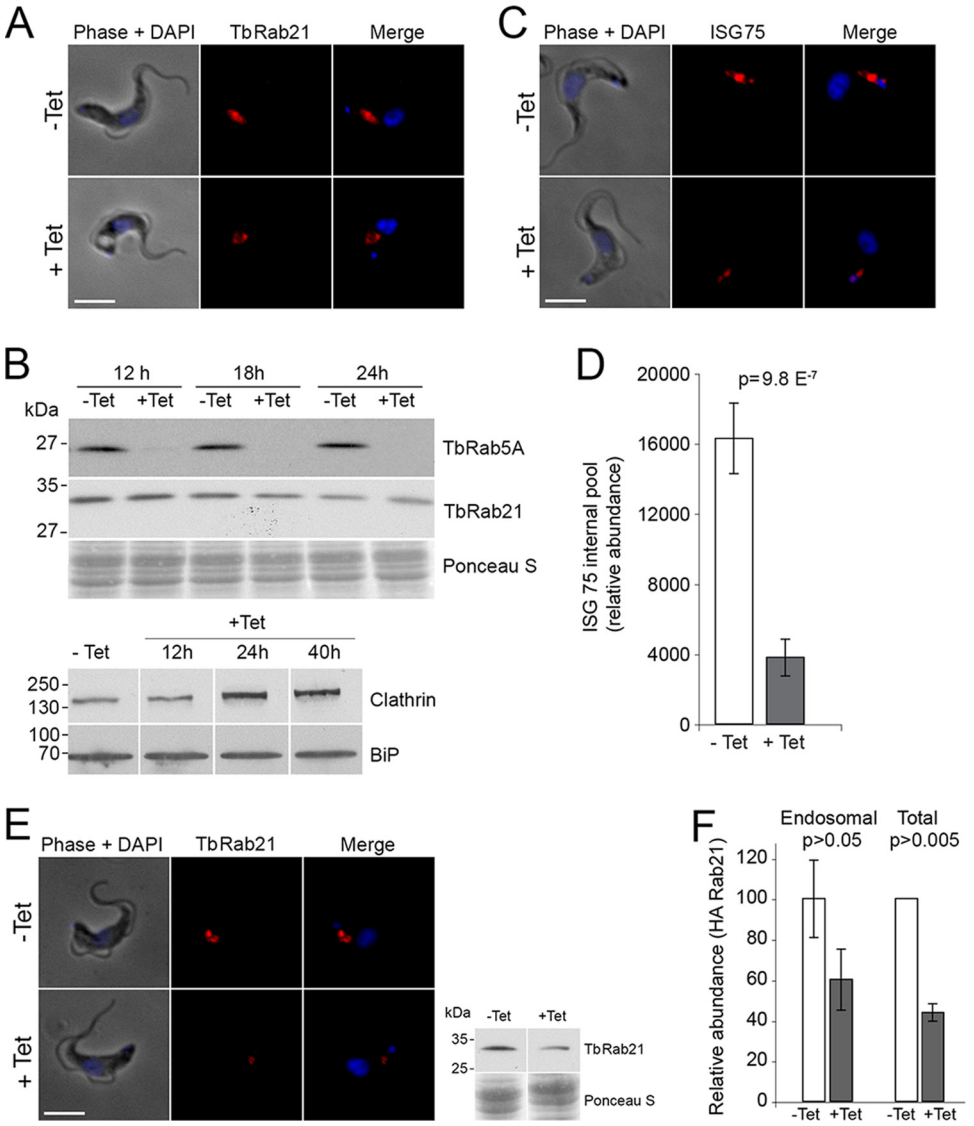

FIG 8 Membrane recruitment of TbRab21 is independent of TbRab5A but depends on TbVps23. (A) BSF TbRab5A knockdown cells were transfected with HA-TbRab21 and induced for 36 h to deplete TbRab5A. Cells were fixed and labeled with monoclonal anti-HA antibodies followed by anti-mouse Alexa Fluor 568-labeled antibodies. DNA was counterstained using DAPI. (B) Western blots showing HA-TbRab21 and TbClathrin, following knockdown of TbRab5A. (C) IFA of the internal pool of ISG75 in TbRab5A RNAi cells. (D) Level of endosomal ISG75 quantified in TbRab5A RNAi cells by IFA. A total of 30 randomly selected induced and uninduced cells were counted under nonsaturating conditions using Metamorph software. (E) TbVps23 knockdown cells expressing recombinant HA-Rab21 and IFA of induced and uninduced cells. (Inset) Total amount of HA-tagged TbRab21 quantified by Western blotting, following knockdown of TbVps23. (F) Quantification of endosomal TbRab21 by IFA and total TbRab21 by Western blotting after 24 h of TbVps23 RNAi treatment. IFA quantification was done by randomly selecting 30 cells each from −Tet (white bars) and +Tet (gray bars) cells and determining HA-Rab21-related fluorescence using Metamorph. +Tet data are expressed as percent −Tet, whereas the error bars denote standard errors of the means. The total quantity of HA-TbRab21 in +Tet cells is plotted as percent −Tet. Student's *t* test showed statistically significant differences in the levels of expression of HA-tagged TbRab21 after TbVps23 knockdown.

blotting. Unexpectedly, a significant reduction in the amount of TbRab21 following 24 h of induction of TbVps23 RNAi was found (Fig. 8E). These data therefore suggest that TbRab21 expression levels are dependent on TbVps23 and indicate an intimate connection between TbRab21, TbRab28, and TbVps23.

DISCUSSION

To extend understanding of the roles of Rab GTPases in *T. brucei*, and to more fully characterize the levels of complexity within the trypanosome endomembrane system and to determine the level of conservation of function of Rab21 across eukaryotes, we investigated the location and functions of trypanosome Rab21. We elected to examine the roles of TbRab21 in turnover of surface proteins as well as in *trans* effects on protein stability in comparisons between TbRab21 and additional components of the trypanosome endomembrane system.

Little is known of Rab21 function in any organism, beyond its being assigned to an early endocytic step and probably acting slightly later than Rab5, together with its influence on the trafficking of several lineage-specific endomembrane/surface proteins

(24, 27, 29). Comparative genomics revealed the presence of Rab21 in members of all eukaryotic supergroups but with many secondary losses, suggesting both an ancient origin and a probable presence in the LECA (21, 61). The vast majority of metazoan species retain Rab21, but it is not found in any of the sequenced fungi or apicomplexans (21, 61). The absence of Rab21 from Apicomplexa is consistent with a general trend of minimization of trafficking components in these parasites (50, 62). Similarly, fungi are also known to encode a limited cohort of Rab proteins in spite of their saprophytic lifestyle and occasional multicellularity (63). Therefore, we suggest that Rab21 is unlikely to mediate a mainline pathway but is more likely to participate in an elaboration or differentiation of a trafficking route.

In trypanosomes, Rab21 was found on both early and late endosomes, partially colocalizing with TbRab5A and with the late endosomal/MVB components TbRab28 and TbVps23. TbRab21 was clearly not present on recycling/exocytic endosomes, the Golgi complex, or the lysosome. While these localization data were insufficient to fully assign TbRab21 to a specific endosomal subpopulation or domain, gene silencing revealed that TbRab21 was indispensable for cell survival. Loss of TbRab21 resulted in a partial prelysosomal blockade to trafficking, as indicated by altered localizations of endocytic cargo molecules with the lysosomal marker p67 and intracellular ISGs. These data are consistent with the *Homo sapiens* Rab21 orthologue, where overexpression of the GTPase-inactive TN mutant resulted in reduced movement of cargo to lysosomes. However, transferrin and ConA uptake following TbRab21 knockdown remained unperturbed, in contrast to overexpression of the *H. sapiens* Rab21 TN mutant, where uptake of transferrin and epidermal growth factor was reduced, suggesting action at earlier steps in the endocytic pathway (22). The recycling of transferrin in TbRab21-depleted BSF cells was also unperturbed, with the results in this case being similar to *H. sapiens* Rab21 TN data (22), suggesting that Rab21 is not involved in recycling of the trypanosome transferrin receptor. Knockdown of TbRab21 also had no effect on TbRab5A but resulted in a decrease in the copy numbers of TbRab28 and TbVps23, late endosomal/MVB components, suggesting that TbRab21 acts downstream of TbRab5A. Note that these in *trans* effects of suppression are not necessarily the result of direct physical interactions with TbRab21 and may be mediated by alterations in the endosomal membrane or effects on shared effector molecules or combinations of these phenomena.

Taken together with earlier work in TbRab5A and -5B, our data suggest that both members of the Rab5 subfamily are essential in *T. brucei*, indicating distinct functions (13). Although TbRab21 is apparently not involved in bulk membrane endocytosis, this GTPase likely provides an important link between the early and late endosomes (Fig. 9). Unfortunately, the early onset of a cytokinesis and proliferative defect following induction of RNAi of TbRab21 limited functional analysis of the endocytic components to an early postinduction time, in most cases earlier than 24 h. Moreover, the secondary effect of TbRab21 knockdown on TbRab28 levels precluded analysis of the effect of TbRab21 depletion on retrograde pathway, as a range of endosomal defects, including retrograde transport, are known following knockdown of TbRab28 (18). TbRab28 depletion disrupts Golgi morphology, reminiscent of retromer component TbVps26 knockdown, but this is not phenocopied in the TbRab21 knockdown (64). Furthermore, TbRab28 knockdown results in loss of the ESCRT-I TbVps23 component, establishing a link between endosomal Rab proteins and the ESCRT (18). The depletion of TbRab21 also resulted in loss of TbVps23, but to a lesser extent than was seen with TbRab28 RNAi, suggesting either an indirect effect via TbRab28 or a direct contribution to the stability of TbVps23. The loss of TbVps23 following the knockdown of TbRab21 likely explains the increase in the intracellular pool of ISGs. The idea of a role for TbVps23 in ISG turnover has been challenged recently (59), but both in this more recent study and in our own earlier work, TbVps23 knockdown was insufficient to robustly protect ISGs from degradation; knockdown of TbVps23 itself protects ISG65 from lysosomal degradation only modestly (50), while protection for ISG75 was statistically insignificant (53), suggesting the possibility of the presence of alternate pathways or of cryptic ubiquitin recognition events within the *T. brucei* ESCRT system that could substitute for Vps23. Moreover, trypanosomes encode a second possible Vps23 orthologue, although in this case the level of conservation with higher eukaryotes is very poor, and the function of this protein has not so far been investigated (50).

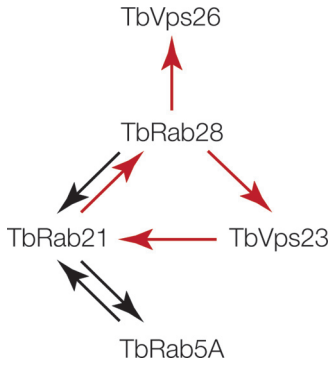

FIG 9 A model linking endosomal Rabs and components of ESCRT and retromer in trypanosomes. Relationships are predicted based on the in *trans* effect on protein copy number following RNA interference. Data represent induction of RNAi against mRNA encoding protein A and assessment of copy numbers of protein B. Arrows indicate the interactions where analysis has been performed, with the arrow pointing from protein A to protein B, and red indicates that the RNAi resulted in decreased copy numbers. Data suggest a complex interplay between TbRab21 and TbRab28 and between ESCRT and retromer but suggest that the network does not extend to the early endocytic TbRab5A. No direct interactions between the proteins mentioned above have currently been demonstrated, and it is unknown how these genetic interactions are mediated at the physical level.

ESCRT components are highly conserved and are shared from Archaea to Metazoa, catalyzing the biogenesis of multivesicular bodies (MVBs) and cytokinesis. On late endosomes, ESCRT components recognize ubiquitinated cargo and sort it into intralumenal vesicles (ILVs) giving the characteristic appearance to MVBs. Compared to mammalian systems, a notable difference in *T. brucei* is the absence of ESCRT-0. ESCRT-0 recruits ESCRT-I, and its absence suggests the presence of an alternative mechanism(s) for ESCRT recruitment (50). Although mechanisms regulating endosome maturation are well understood (65), the connections with the ESCRT system remains elusive. SAND-1/Mon1 is an important regulatory molecule for conversion of Rab5 to Rab7 and is capable of timing this event by recognizing PI(3)P, as shown by disruption of SAND-1/Mon1 endosomal binding in the presence of the PI(3)K inhibitor wortmannin (66). This timing is important, as Rab conversion should happen after the accumulation of ubiquitinated cargo in ILVs of late endosomes. But this timing

mechanism is not sufficient to regulate ILV formation, as the overexpression of a GTP-locked Rab5 QL mutant does not affect cargo sorting or ILV formation (67). Furthermore, Rab7-depleted cells also form ILVs (68). Therefore, neither inactivation of Rab5 nor the arrival of Rab7 is sufficient to coordinate MVB formation. *T. brucei* Rab28 affects the ESCRT-I component TbVps23 (18), and results presented here further elaborate this interaction, where RNAi knockdown of TbRab21 resulted in the loss of both TbRab28 and TbVps23, while knockdown of TbVps23 resulted in decreased TbRab21 protein expression. Taken together, these data suggest that Rab21 and Rab28 could possibly synchronize the ESCRT assembly/MVB biogenesis and retrograde transport with endosome maturation. This Rab-ESCRT relationship is presently indirect, and no direct molecular link has been identified. It can be speculated that an effector of TbRab21 or TbRab28 interacts with ESCRT molecules. A similar role is known for Rab7 effector RILP, which is required for ILV formation and also interacts with ESCRT-II (69). The existence of such an effector of TbRab21 that can interact with ESCRT could also explain the loss of TbRab21 following the depletion of TbVps23, as effectors also stabilize their Rabs in the active form. Clearly, more work is needed in this area to fully chart the role of ESCRT and Rab proteins in late endocytosis in trypanosomes and to confirm whether the mechanisms at play here are fully shared with mammalian cells.

The presence of TbRab21 at the late endosome adds to the complexity of the degradative arm of the trypanosome endocytic system, which is now known to require at least six Rab GTPases (Rab4, Rab5A, Rab5B, Rab7, Rab21, and Rab28) for correct functioning. Interactions with a growing number of non-Rab components of the ESCRT and retromer systems are being identified, and mapping the evolution of regulation of these GTPases will clearly be an important goal for understanding how Rabs have contributed to the sculpting of the eukaryotic endomembrane system.

ACKNOWLEDGMENTS

This work was supported by a Wellcome Trust program grant (082813 to M.C.F.) and a scholarship from the Higher Education Commission, Pakistan (to M.A.).

We are grateful to the following for the gift of various reagents: James Bangs (Buffalo) for antibodies to TbBiP and p67 and Piet Borst (Amsterdam) for antibody against the transferrin receptor. We are also grateful to members of our laboratory for comments on the manuscript.

REFERENCES

1. **Field MC, Carrington M.** 2009. The trypanosome flagellar pocket. Nat. Rev. Microbiol. **7:**775–786. http://dx.doi.org/10.1038/nrmicro2221.
2. **Allen CL, Goulding D, Field MC.** 2003. Clathrin-mediated endocytosis is essential in *Trypanosoma brucei*. EMBO J. **22:**4991–5002. http://dx.doi.org/10.1093/emboj/cdg481.
3. **Manna P, Kelly S, Field MC.** 2013. Co-evolution of antigenic variation and adaptins in trypanosomatids. Mol. Protein Evol. **67:**123–128.
4. **Adung'a VO, Gadelha C, Field MC.** 2013. Proteomic analysis of clathrin interactions in trypanosomes reveals dynamic evolution of endocytosis. Traffic **14:**440–457. http://dx.doi.org/10.1111/tra.12040.
5. **Engstler M, Pfohl T, Herminghaus S, Boshart M, Wiegertjes G, Heddergott N, Overath P.** 2007. Hydrodynamic flow-mediated protein sorting on the cell surface of trypanosomes. Cell **131:**505–515. http://dx.doi.org/10.1016/j.cell.2007.08.046.
6. **Vanhollebeke B, Pays E.** 2010. The trypanolytic factor of human serum: many ways to enter the parasite, a single way to kill. Mol. Microbiol. **76:**806–814. http://dx.doi.org/10.1111/j.1365-2958.2010.07156.x.
7. **Uzureau P, Uzureau S, Lecordier L, Fontaine F, Tebabi P, Homblé F, Grélard A, Zhendre V, Nolan DP, Lins L, Crowet JM, Pays A, Felu C, Poelvoorde P, Vanhollebeke B, Moestrup SK, Lyngsø J, Pedersen JS, Mottram JC, Dufourc EJ, Pérez-Morga D, Pays E.** 21 August 2013. Mechanism of *Trypanosoma brucei gambiense* resistance to human serum. Nature http://dx.doi.org/10.1038/nature12516.
8. **Alsford S, Eckert S, Baker N, Glover L, Sanchez-Flores A, Leung KF, Turner DJ, Field MC, Berriman M, Horn D.** 2012. High-throughput decoding of antitrypanosomal drug efficacy and resistance. Nature **482:**232–236. http://dx.doi.org/10.1038/nature10771.
9. **Alsford S, Field MC, Horn D.** 2013. Receptor-mediated endocytosis for drug delivery in African trypanosomes. Trends Parasitol. **29:**207–212. http://dx.doi.org/10.1016/j.pt.2013.03.004.
10. **Stenmark H.** 2009. Rab GTPases as coordinators of vesicle traffic. Nat. Rev. Mol. Cell Biol. **10:**513–525. http://dx.doi.org/10.1038/nrm2728.
11. **Jeffries TR, Morgan GW, Field MC.** 2001. A developmentally regulated rab11 homologue in *Trypanosoma brucei* is involved in recycling processes. J. Cell Sci. **114**(Pt 14)**:**2617–2626.
12. **Pal A, Hall BS, Jeffries TR, Field MC.** 2003. Rab5 and Rab11 mediate transferrin and anti-variant surface glycoprotein antibody recycling in *Trypanosoma brucei*. Biochem. J. **374:**443–451. http://dx.doi.org/10.1042/BJ20030469.
13. **Hall B, Allen CL, Goulding D, Field MC.** 2004. Both of the Rab5 subfamily small GTPases of *Trypanosoma brucei* are essential and required for endocytosis. Mol. Biochem. Parasitol. **138:**67–77. http://dx.doi.org/10.1016/j.molbiopara.2004.07.007.
14. **Hall BS, Pal A, Goulding D, Acosta-Serrano A, Field MC.** 2005. Trypanosoma brucei: TbRAB4 regulates membrane recycling and expression of surface proteins in procyclic forms. Exp. Parasitol. **111:**160–171. http://dx.doi.org/10.1016/j.exppara.2005.07.005.
15. **Hall BS, Pal A, Goulding D, Field MC.** 2004. Rab4 is an essential regulator of lysosomal trafficking in trypanosomes. J. Biol. Chem. **279:**45047–45056. http://dx.doi.org/10.1074/jbc.M407271200.
16. **Hall BS, Smith E, Langer W, Jacobs LA, Goulding D, Field MC.** 2005. Developmental variation in Rab11-dependent trafficking in *Trypanosoma brucei*. Eukaryot. Cell **4:**971–980. http://dx.doi.org/10.1128/EC.4.5.971-980.2005.
17. **Grünfelder CG, Engstler M, Weise F, Schwarz H, Stierhof YD, Morgan GW, Field MC, Overath P.** 2003. Endocytosis of a glycosylphosphatidylinositol-anchored protein via clathrin-coated vesicles, sorting by default in endosomes, and exocytosis via RAB11-positive carriers. Mol. Biol. Cell **14:**2029–2040. http://dx.doi.org/10.1091/mbc.E02-10-0640.
18. **Lumb JH, Leung KF, Dubois KN, Field MC.** 2011. Rab28 function in trypanosomes: interactions with retromer and ESCRT pathways. J. Cell Sci. **124:**3771–3783. http://dx.doi.org/10.1242/jcs.079178.
19. **Silverman JS, Schwartz KJ, Hajduk SL, Bangs JD.** 2011. Late endosomal Rab7 regulates lysosomal trafficking of endocytic but not biosynthetic cargo in *Trypanosoma brucei*. Mol. Microbiol. **82:**664–678. http://dx.doi.org/10.1111/j.1365-2958.2011.07842.x.
20. **Ackers JP, Dhir V, Field MC.** 2005. A bioinformatic analysis of the RAB genes of *Trypanosoma brucei*. Mol. Biochem. Parasitol. **141:**89–97. http://dx.doi.org/10.1016/j.molbiopara.2005.01.017.
21. **Elias M, Brighouse A, Gabernet-Castello C, Field MC, Dacks JB.** 2012. Sculpting the endomembrane system in deep time: high resolution phylogenetics of Rab GTPases. J. Cell Sci. **125:**2500–2508. http://dx.doi.org/10.1242/jcs.101378.
22. **Simpson JC, Griffiths G, Wessling-Resnick M, Fransen JA, Bennett H, Jones AT.** 2004. A role for the small GTPase Rab21 in the early endocytic pathway. J. Cell Sci. **117:**6297–6311. http://dx.doi.org/10.1242/jcs.01560.
23. **Opdam FJ, Kamps G, Croes H, Van Bokhoven H, Ginsel LA, Fransen JA.** 2000. Expression of Rab small GTPases in epithelial Caco-2 cells: Rab21 is an apically located GTP-binding protein in polarised intestinal epithelial cells. Eur. J. Cell Biol. **79:**308–316. http://dx.doi.org/10.1078/S0171-9335(04)70034-5.
24. **Khurana T, Brzostowski JA, Kimmel AR.** 2005. A Rab21/LIM-only/CH-LIM complex regulates phagocytosis via both activating and inhibitory mechanisms. EMBO J. **24:**2254–2264. http://dx.doi.org/10.1038/sj.emboj.7600716.
25. **Egami Y, Araki N.** 2008. Characterization of Rab21-positive tubular endosomes induced by PI3K inhibitors. Exp. Cell Res. **314:**729–737. http://dx.doi.org/10.1016/j.yexcr.2007.11.018.
26. **Egami Y, Araki N.** 2009. Dynamic changes in the spatiotemporal localization of Rab21 in live RAW264 cells during macropinocytosis. PLoS One **4:**e6689. http://dx.doi.org/10.1371/journal.pone.0006689.
27. **Pellinen T, Tuomi S, Arjonen A, Wolf M, Edgren H, Meyer H, Grosse R, Kitzing T, Rantala JK, Kallioniemi O, Fassler R, Kallio M, Ivaska J.**

2008. Integrin trafficking regulated by Rab21 is necessary for cytokinesis. Dev. Cell **15:**371–385. http://dx.doi.org/10.1016/j.devcel.2008.08.001.
28. **Pellinen T, Arjonen A, Vuoriluoto K, Kallio K, Fransen JA, Ivaska J.** 2006. Small GTPase Rab21 regulates cell adhesion and controls endosomal traffic of beta1-integrins. J. Cell Biol. **173:**767–780. http://dx.doi.org/10.1083/jcb.200509019.
29. **Mai A, Veltel S, Pellinen T, Padzik A, Coffey E, Marjomaki V, Ivaska J.** 2011. Competitive binding of Rab21 and p120RasGAP to integrins regulates receptor traffic and migration. J. Cell Biol. **194:**291–306. http://dx.doi.org/10.1083/jcb.201012126.
30. **Pellinen T, Ivaska J.** 2006. Integrin traffic. J. Cell Sci. **119:**3723–3731. http://dx.doi.org/10.1242/jcs.03216.
31. **Caswell PT, Vadrevu S, Norman JC.** 2009. Integrins: masters and slaves of endocytic transport. Nat. Rev. Mol. Cell Biol. **10:**843–853. http://dx.doi.org/10.1038/nrm2799.
32. **Hirumi H, Hirumi K.** 1989. Continuous cultivation of *Trypanosoma brucei* blood stream forms in a medium containing a low concentration of serum protein without feeder cell layers. J. Parasitol. **75:**985–989. http://dx.doi.org/10.2307/3282883.
33. **Wirtz E, Leal S, Ochatt C, Cross GA.** 1999. A tightly regulated inducible expression system for conditional gene knock-outs and dominant-negative genetics in *Trypanosoma brucei*. Mol. Biochem. Parasitol. **99:**89–101. http://dx.doi.org/10.1016/S0166-6851(99)00002-X.
34. **Brun R, Schönenberger J.** 1979. Cultivation and in vitro cloning or procyclic culture forms of *Trypanosoma brucei* in a semi-defined medium. Short communication. Acta Trop. **36:**289–292.
35. **Field MC, Horn D, Carrington M.** 2008. Analysis of small GTPase function in trypanosomes. Methods Enzymol. **438:**57–76. http://dx.doi.org/10.1016/S0076-6879(07)38005-1.
36. **LaCount DJ, Barrett B, Donelson JE.** 2002. Trypanosoma brucei FLA1 is required for flagellum attachment and cytokinesis. J. Biol. Chem. **277:**17580–17588. http://dx.doi.org/10.1074/jbc.M200873200.
37. **Quijada L, Guerra-Giraldez C, Drozdz M, Hartmann C, Irmer H, Ben-Dov C, Cristodero M, Ding M, Clayton C.** 2002. Expression of the human RNA-binding protein HuR in *Trypanosoma brucei* increases the abundance of mRNAs containing AU-rich regulatory elements. Nucleic Acids Res. **30:**4414–4424. http://dx.doi.org/10.1093/nar/gkf577.
38. **Brenndörfer M, Boshart M.** 2010. Selection of reference genes for mRNA quantification in *Trypanosoma brucei*. Mol. Biochem. Parasitol. **172:**52–55. http://dx.doi.org/10.1016/j.molbiopara.2010.03.007.
39. **Nolan DP, Jackson DG, Biggs MJ, Brabazon ED, Pays A, Van Laethem F, Paturiaux-Hanocq F, Elliott JF, Voorheis HP, Pays E.** 2000. Characterization of a novel alanine-rich protein located in surface microdomains in *Trypanosoma brucei*. J. Biol. Chem. **275:**4072–4080. http://dx.doi.org/10.1074/jbc.275.6.4072.
40. **Morgan GW, Allen CL, Jeffries TR, Hollinshead M, Field MC.** 2001. Developmental and morphological regulation of clathrin-mediated endocytosis in *Trypanosoma brucei*. J. Cell Sci. **114**(Pt 14)**:**2605–2615.
41. **Pal A, Hall BS, Nesbeth DN, Field HI, Field MC.** 2002. Differential endocytic functions of *Trypanosoma brucei* Rab5 isoforms reveal a glycosylphosphatidylinositol-specific endosomal pathway. J. Biol. Chem. **277:**9529–9539. http://dx.doi.org/10.1074/jbc.M110055200.
42. **Natesan SK, Peacock L, Leung KF, Matthews KR, Gibson W, Field MC.** 2009. The trypanosome Rab-related proteins RabX1 and RabX2 play no role in intracellular trafficking but may be involved in fly infectivity. PLoS One **4:**e7217. http://dx.doi.org/10.1371/journal.pone.0007217.
43. **Ziegelbauer K, Multhaup G, Overath P.** 1992. Molecular characterization of two invariant surface glycoproteins specific for the bloodstream stage of *Trypanosoma brucei*. J. Biol. Chem. **267:**10797–10803.
44. **Bangs JD, Uyetake L, Brickman MJ, Balber AE, Boothroyd JC.** 1993. Molecular cloning and cellular localization of a BiP homologue in *Trypanosoma brucei*. Divergent ER retention signals in a lower eukaryote. J. Cell Sci. **105**(Pt 4)**:**1101–1113.
45. **Gerrits H, Mussmann R, Bitter W, Kieft R, Borst P.** 2002. The physiological significance of transferrin receptor variations in Trypanosoma brucei. Mol. Biochem. Parasitol. **119:**237–247. http://dx.doi.org/10.1016/S0166-6851(01)00417-0.
46. **Kelley RJ, Alexander DL, Cowan C, Balber AE, Bangs JD.** 1999. Molecular cloning of p67, a lysosomal membrane glycoprotein from *Trypanosoma brucei*. Mol. Biochem. Parasitol. **98:**17–28. http://dx.doi.org/10.1016/S0166-6851(98)00155-8.
47. **Koumandou VL, Natesan SK, Sergeenko T, Field MC.** 2008. The trypanosome transcriptome is remodelled during differentiation but displays limited responsiveness within life stages. BMC Genomics **9:**298. http://dx.doi.org/10.1186/1471-2164-9-298.
48. **Siegel TN, Hekstra DR, Wang X, Dewell S, Cross GA.** 2010. Genome-wide analysis of mRNA abundance in two life-cycle stages of *Trypanosoma brucei* and identification of splicing and polyadenylation sites. Nucleic Acids Res. **38:**4946–4957. http://dx.doi.org/10.1093/nar/gkq237.
49. **Lumb JH, Field MC.** 2011. Rab23 is a flagellar protein in *Trypanosoma brucei*. BMC Res. Notes **4:**190. http://dx.doi.org/10.1186/1756-0500-4-190.
50. **Leung KF, Dacks JB, Field MC.** 2008. Evolution of the multivesicular body ESCRT machinery; retention across the eukaryotic lineage. Traffic **9:**1698–1716. http://dx.doi.org/10.1111/j.1600-0854.2008.00797.x.
51. **Field H, Farjah M, Pal A, Gull K, Field MC.** 1998. Complexity of trypanosomatid endocytosis pathways revealed by TbRab5 isoforms in *Trypanosoma brucei*. J. Biol. Chem. **273:**32102–32110. http://dx.doi.org/10.1074/jbc.273.48.32102.
52. **Field H, Field MC.** 1997. Tandem duplication of rab genes followed by sequence divergence and acquisition of distinct functions in *Trypanosoma brucei*. J. Biol. Chem. **272:**10498–10508. http://dx.doi.org/10.1074/jbc.272.16.10498.
53. **Field H, Sherwin T, Smith AC, Gull K, Field MC.** 2000. Cell-cycle and developmental regulation of TbRAB31 localisation, a GTP-locked Rab protein from *Trypanosoma brucei*. Mol. Biochem. Parasitol. **106:**21–35. http://dx.doi.org/10.1016/S0166-6851(99)00192-9.
54. **Peck RF, Shiflett AM, Schwartz KJ, Mccann A, Hajduk SL, Bangs JD.** 2008. The LAMP-like protein p67 plays an essential role in the lysosome of African trypanosomes. Mol. Microbiol. **68:**933–946. http://dx.doi.org/10.1111/j.1365-2958.2008.06195.x.
55. **Ali M, Field MC.** 2013. Cell density-dependent ectopic expression in bloodstream form *Trypanosoma brucei*. Exp. Parasitol. **134:**249–255. http://dx.doi.org/10.1016/j.exppara.2013.03.017.
56. **Borst P, Fairlamb AH.** 1998. Surface receptors and transporters of *Trypanosoma brucei*. Annu. Rev. Microbiol. **52:**745–778. http://dx.doi.org/10.1146/annurev.micro.52.1.745.
57. **Chung WL, Leung KF, Carrington M, Field MC.** 2008. Ubiquitylation is required for degradation of transmembrane surface proteins in trypanosomes. Traffic **9:**1681–1697. http://dx.doi.org/10.1111/j.1600-0854.2008.00785.x.
58. **Fast B, Kremp K, Boshart M, Steverding D.** 1999. Iron-dependent regulation of transferrin receptor expression in *Trypanosoma brucei*. Biochem. J. **342**(Pt 3)**:**691–696. http://dx.doi.org/10.1042/0264-6021:3420691.
59. **Silverman JS, Muratore KA, Bangs JD.** 18 August 2013. Characterization of the late endosomal ESCRT machinery in *Trypanosoma brucei*. Traffic http://dx.doi.org/10.1111/tra.12094.
60. **Brighouse A, Dacks JB, Field MC.** 2010. Rab protein evolution and the history of the eukaryotic endomembrane system. Cell. Mol. Life Sci. **67:**3449–3465. http://dx.doi.org/10.1007/s00018-010-0436-1.
61. **Diekmann Y, Seixas E, Gouw M, Tavares-Cadete F, Seabra MC, Pereira-Leal JB.** 2011. Thousands of rab GTPases for the cell biologist. PLoS Comput. Biol. **7:**e1002217. http://dx.doi.org/10.1371/journal.pcbi.1002217.
62. **Koumandou VL, Dacks JB, Coulson RM, Field MC.** 2007. Control systems for membrane fusion in the ancestral eukaryote; evolution of tethering complexes and SM proteins. BMC Evol. Biol. **7:**29. http://dx.doi.org/10.1186/1471-2148-7-29.
63. **Pereira-Leal JB.** 2008. The Ypt/Rab family and the evolution of trafficking in fungi. Traffic **9:**27–38. http://dx.doi.org/10.1111/j.1600-0854.2007.00667.x.
64. **Koumandou VL, Klute MJ, Herman EK, Nunez-Miguel R, Dacks JB, Field MC.** 2011. Evolutionary reconstruction of the retromer complex and its function in *Trypanosoma brucei*. J. Cell Sci. **124:**1496–1509. http://dx.doi.org/10.1242/jcs.081596.
65. **Huotari J, Helenius A.** 2011. Endosome maturation. EMBO J. **30:**3481–3500. http://dx.doi.org/10.1038/emboj.2011.286.
66. **Poteryaev D, Datta S, Ackema K, Zerial M, Spang A.** 2010. Identification of the switch in early-to-late endosome transition. Cell **141:**497–508. http://dx.doi.org/10.1016/j.cell.2010.03.011.
67. **Wegner CS, Malerod L, Pedersen NM, Progida C, Bakke O, Stenmark H, Brech A.** 2010. Ultrastructural characterization of giant endosomes induced by GTPase-deficient Rab5. Histochem. Cell Biol. **133:**41–55. http://dx.doi.org/10.1007/s00418-009-0643-8.
68. **Vanlandingham PA, Ceresa BP.** 2009. Rab7 regulates late endocytic trafficking downstream of multivesicular body biogenesis and cargo seques-

tration. J. Biol. Chem. **284:**12110–12124. http://dx.doi.org/10.1074/jbc.M809277200.
69. **Progida C, Malerod L, Stuffers S, Brech A, Bucci C, Stenmark H.** 2007. RILP is required for the proper morphology and function of late endosomes. J. Cell Sci. **120:**3729–3737. http://dx.doi.org/10.1242/jcs.017301.
70. **Leung KF, Riley FS, Carrington M, Field MC.** 2011. Ubiquitylation and developmental regulation of invariant surface protein expression in trypanosomes. Eukaryot. Cell **10:**916–931. http://dx.doi.org/10.1128/EC.05012-11.
71. **Overath P, Engstler M.** 2004. Endocytosis, membrane recycling and sorting of GPI-anchored proteins: Trypanosoma brucei as a model system. Mol. Microbiol. **53:**735–744. http://dx.doi.org/10.1111/j.1365-2958.2004.04224.x.
72. **Gabernet-Castello C, Dacks JB, Field MC.** 2009. The single ENTH-domain protein of trypanosomes; endocytic functions and evolutionary relationship with epsin. Traffic **10:**894–911. http://dx.doi.org/10.1111/j.1600-0854.2009.00910.x.
73. **Kabiri M, Steverding D.** 2000. Studies on the recycling of the transferrin receptor in Trypanosoma brucei using an inducible gene expression system. Eur. J. Biochem. **267:**3309–3314. http://dx.doi.org/10.1046/j.1432-1327.2000.01361.x.